Accurate determination of the size distribution for polydisperse, cationic metallic nanomaterials by asymmetric-flow field flow fractionation

ARTICLE *in* JOURNAL OF NANOPARTICLE RESEARCH · NOVEMBER 2014

Impact Factor: 2.18 · DOI: 10.1007/s11051-014-2735-1

J Nanopart Res (2014) 16:2735
DOI 10.1007/s11051-014-2735-1

RESEARCH PAPER

Accurate determination of the size distribution for polydisperse, cationic metallic nanomaterials by asymmetric-flow field flow fractionation

Julien Gigault · Thao M. Nguyen · John M. Pettibone · Vincent A. Hackley

Received: 5 September 2014 / Accepted: 4 November 2014

Abstract In this work we have developed and validated a methodology for determining the size distribution in polydisperse cationic nanoparticle (NP) samples using asymmetric-flow field flow fractionation (A4F), where known compositional influence of previously used calibrants was mitigated. Both the accurate determination of NP size distributions, in general, and the evaluation of cationic species with A4F have proved to be persistent analytical challenges, especially for strong, optically absorbing metallic NPs. In order to overcome these challenges, highly uniform and monomodal cetyl trimethylammonium bromide (CTAB)-stabilized SeNPs were prepared through a facile synthetic procedure and were further validated as an appropriate calibrant for cationic gold NPs based on their inherent optical properties and (nearly) identical retention behavior. Due to the uniform retention behavior resulting from the NP coating and narrow distribution ($\sigma_d \ll$ diameter) of the calibrant, the contributions from sample polydispersity and instrumental broadening of the theoretical plate height, H, could be isolated and the size distribution determined. Although this has been demonstrated previously for macromolecules, to our knowledge the size distribution has not been reported and validated for NP analytes. Implementation of the calibrant in a polydisperse CTAB-coated AuNP sample demonstrates the capabilities of the current method and could be easily extended to other systems. Overall, the necessity of robust methods for size distribution determination are currently addressed that incorporate appropriate calibrants when light scattering methods are intractable, providing an alternative method in systems that are difficult with traditional microscopy approaches.

Keywords Nanoparticle · Field flow fractionation · Selenium · Gold · CTAB · Calibration standard · Size characterization

Electronic supplementary material The online version of this article (doi:10.1007/s11051-014-2735-1) contains supplementary material, which is available to authorized users.

J. Gigault (✉) · T. M. Nguyen · J. M. Pettibone · V. A. Hackley
Materials Measurement Science Division, National Institute of Standards and Technology, 100 Bureau Drive, Gaithersburg, MD 20899-8520, USA
e-mail: julien.gigault@u-bordeaux.fr

Present Address:
J. Gigault
Laboratoire de Physico- et Toxico-Chimie de l'Environnement, Centre National de la Recherche Scientifique (CNRS), 351 Cours de la Libération, Talence 33405, France

Introduction

Positively charged nanoparticles (NPs) have properties that herald a promising future and are becoming more relevant to biomedical applications, for instance,

Published online: 13 November 2014

in the field of nano-medicine (Gill and Lucassen 2010; Ma et al. 2009; van Lierop et al. 2012). Among the most commonly employed materials are noble metals, metal oxides, and polymeric materials. Processing of these materials often yields a distribution of products and product dimensions that require significant purification or secondary processing, especially metallic species. A lack of tools for characterizing the product distribution has also hindered the further development of nanomaterial based products. Overall, characterization of a broad range of NP compositions, sizes, and shapes, especially in complex solution-phase systems inducing growth or transformation, continues to be a persistent analytical challenge (Brown et al. 2013; Gigault and Hackley 2013; Hassellöv et al. 2008; Howard 2010; von der Kammer et al. 2011; Pettibone et al. 2013; Sapsford et al. 2011; Wei et al. 2012).

Field flow fractionation offers a versatile class of methods for size separation and characterization of species in the nanoscale-to-microscale regime (Giddings 1984; Giddings et al. 1983, 1976a, 1976b). The separation mechanism is based on the diffusion of the analytes, not on the direct interaction with a stationary phase (as in traditional chromatographic techniques), and has resulted in the successful fractionation of a variety of nanomaterials with distinct shapes and surface properties. Accurate characterization of the *mean* diffusion coefficient (determined by size) based on retention with asymmetric-flow field flow fractionation (A4F) is an increasingly common procedure applied to nanomaterials, particularly when hyphenation of A4F with light scattering measurements is problematic due to inefficient and/or complex scattering of the sample (e.g., size, concentration, or optical properties). For example, metallic NPs exhibiting plasmon resonances, such as Au and Ag, do not exhibit simple angular-dependent scattering, resulting in the inability to characterize the size or shape of the nanomaterials with static light scattering (SLS) methods. Therefore, accurate calibration of the diffusion-based retention becomes imperative, and the use of appropriate methods must be validated.

To develop and validate such a method, accurate standardized calibration materials with known physico-chemical properties are also necessary. A common practice for calibrating diffusion is the use of well-characterized, commercially available polymer latices (typically polystyrene spheres), where interaction between the membrane and the calibrant or analyte of interest are assumed to be similar based on surface charge (e.g., zeta potential) in known ionic strength, I, media. However, even though surface properties of the calibrant and NP analyte are similar, previous work has shown that compositional influences also strongly contribute to the retention behavior in the channel and can result in inaccurate determination of analyte diffusion and therefore size (Gigault and Hackley 2013; Noskov et al. 2013). The observed compositional influences highlight the importance of incorporating validated methods for calibration.

The importance of understanding the retention behavior and diffusion calibration is magnified for positively charged nanomaterials because of the necessity to modify either the membrane or the mobile phase for optimal fractionation (Bendixen et al. 2014; Lee et al. 2010; Losert et al. 2013; Schimpf et al. 2000). Commercial positively charged membranes are not available at the present time, resulting in the need to modify the mobile phase as previously outlined (Schimpf et al. 2000). It is imperative to examine and understand possible effects on the integrity of both the calibrant and the NP analyte due to additives in the mobile phase. Appropriate calibrants with well-characterized physico-chemical properties that are directly linked to their retention behavior (i.e., retention ratio, $R = t_0/t_R$, where t_0 and t_R are the measured void time and analyte retention time, respectively), can then be confidently employed. The calibrant material should ideally have optical properties that allow for both quantification and characterization with an SLS detector according to their size and shape, while exhibiting uniformity and a narrow size dispersity ($\sigma_d \leq 1$ %). Furthermore, non-interacting calibrants are required, especially in the case of nanoparticles, which present physical properties (magnetic, electrical, etc.) that can impact their associative behavior in solution.

In order to determine size/shape of a polydisperse population, further investigation of the contributing factors to retention and peak broadening must be incorporated, which again requires a (nearly) uniform calibrant with similar retention behavior to the analytes of interest. Determination of the size distribution of NPs is not commonly achieved with A4F in systems where LS measurements cannot be confidently made, and instead, generally a mean size is reported based on t_R at the peak maximum (see Electronic Supplemental Information—ESM, Eq. S1,

for relationship between t_R and the particle diffusion coefficient, D). Accurate determination of polydisperse NP samples, especially relevant to complex systems, has relied on microscopy (scanning probe and electron) to statistically interrogate the entire distribution and requires significant resources. However, as with all measurements performed outside of the sample's native environment, the results may potentially be impacted by sample preparation artifacts (i.e., samples can be sensitive to drying or other ambient environmental conditions) (Glover et al. 2011, Hutchison 2008). These potential pitfalls prompt the development of alternative methods for accurate determination of these materials in their native environment with minimal perturbation.

Based on the inherent optical properties of selenium (strong scattering due to high refractive index −2.64 at a wavelength of 658 nm; lack of surface plasmon resonance effects) and the previously reported capacity to synthesize highly uniform monomodal populations of spherical NPs over a broad size range (Zhang et al. 2004), selenium NPs (SeNPs) were evaluated on their merit as a potential calibrant for size and polydispersity in A4F. In this study, we show that SeNPs can be utilized for the calibration of positively charged metallic species based on retention, t_R, and SLS measurements. Because the quality of the SeNPs in terms of uniformity in size and shape is high, the contributions due to instrumental broadening in the channel can be quantified. Here, instrumental broadening captures contributions to broadening that are not directly attributed to the size dispersion of the analyte (e.g., operational conditions, non-equilibrium effects, etc.). This can in turn be used to elucidate information regarding the relative distribution (standard deviation of the size, σ_d, and polydispersity) present for each unknown population that is fractionated in the A4F channel. Therefore, the development of a fast, reliable, size- and charge-specific A4F method for positively charged NPs is presented and validated. Application of the validation approach to a previously difficult polydisperse cetyl trimethylammonium bromide (CTAB)-coated AuNP material is demonstrated. This study, in conjunction with our previous research (Gigault et al. 2012), suggests applicability of the optimized conditions for a broad range of samples that would include other metallic NPs and non-spherical shapes. However, further validation would be necessary to firmly establish this broad applicability.

Experimental

Chemicals

Ammonium nitrate (NH_4NO_3, 99.5 %), sodium selenite (Na_2SeO_3, 99.9 %), cetyl trimethylammonium bromide (CTAB, 99 %), and ascorbic acid (>99.5 %) were purchased from VWR (Bridgeport, NJ).[1] Gold (III) chloride trihydrate ($HAuCl_4$, ≥ 99.9 %), sodium borohydride ($NaBH_4$, 99.99 %), and sodium hydroxide (NaOH, 97 %) were obtained from Sigma-Aldrich (St. Louis, MO). Deionized (DI) water (18 MΩ cm) used in all experiments was generated by a biological-grade water purification system from Aqua Solutions (Jasper, GA). All A4F mobile phases were passed through a 0.2 μm regenerated cellulose filter from VWR.

Selenium nanoparticle synthesis

Using a previously reported method (Zhang et al. 2004), a broad size range of SeNPs was synthesized using, conjointly, ascorbic acid ($C_6H_8O_6$) as the reducing agent and CTAB as the stabilizing agent; this procedure reportedly results in uniform spherical NPs due to the bi-micellar structure of CTAB. Typically 8 mL of ascorbic acid at 60 mmol L^{-1} was mixed with 1 mL of CTAB at varying concentrations from 0.01 to 30 mmol L^{-1}. Subsequently, 1 mL of 25 mmol L^{-1} Na_2SeO_3 was slowly added drop wise, with vigorous stirring at room temperature. An orange-red color appeared after the initial addition of Na_2SeO_3. Following addition of Na_2SeO_3, the solution was vigorously stirred for several minutes, until there was no visual change in color. Different size SeNPs were obtained simply by controlling the CTAB concentration. Excess CTAB and unreacted Na_2SeO_3 were removed and the particles concentrated by centrifugal filtration (10 kDa MWCO) at 5,000 rpm (83.3 Hz) for 5 min; this procedure was repeated three times. The SeNP concentrate was then resuspended in the A4F mobile phase at the desired concentration. No change in size was observed using this purification process.

[1] The identification of any commercial product or trade name does not imply endorsement or recommendation by the National Institute of Standards and Technology.

Gold NPs were prepared as previously described with slight modifications (Vigderman et al. 2012). A solution of 50 mmol L^{-1} $NaBH_4$ dissolved in 50 mmol L^{-1} NaOH was freshly prepared. Under rapid stirring, 500 μL of the $NaBH_4$ aqueous solution was added to a 5 mL solution containing 50 mmol L^{-1} $HAuCl_4$ and 0.1 mol L^{-1} CTAB. The stirring was terminated after the solution turned light brown in color. In order to obtain a polydisperse mixture of larger gold NPs, the seed solution was heated for 1 h, yielding particles up to approximately 25 nm in diameter.

Instrumentation

The A4F system used in this study consists of an Eclipse 3 + (Wyatt Technology, Santa Barbara, CA) coupled to an Agilent Technologies (Santa Clara, CA) 1100 series isocratic pump, a degasser (Gastorr TG-14, Flom Co., Ltd., Tokyo, Japan), and a manual injector (Rheodyne 7725i, IDEX Corporation, Oak Harbor, WA) with a 100 μL stainless steel sample loop. The detection chain consists of a UV/Vis absorbance diode array detector (DAD, 1200 series, Agilent Technologies) with a spectral range from 190 to 950 nm and a sampling rate of 20 Hz, and a multi-angle light scattering (MALS) detector (DAWN HELEOS, Wyatt Technology) equipped with a fiber optic dynamic light scattering (DLS) sensor (DynaPro, Wyatt Technology). Data from the different detectors was collected and treated with Astra 5.3.1.18 software (Wyatt Technology). The channel spacer was 250 μm and the trapezoidal channel dimensions were 26.5 cm in length and from 2.1 to 0.6 cm in width. For all experiments, polyethersulfone (PES) membranes with a 10 kDa cut-off (Wyatt Technology) were used to define the semi-permeable accumulation wall. In this study, considering the size range of analytes, the channel flow (V_p) was fixed at 0.5 mL min^{-1}.

Transmission electron microscopy (TEM) measurements were performed using a JEM 3010 from JEOL USA Inc. (Peabody, MA, USA). A voltage of 300 kV was used for all samples. TEM sample preparation was performed by purifying analytes with centrifugation and pipetting 10 μL of NP suspension onto a lacey carbon-coated copper TEM grid (Electron Microscopy Sciences, Hatfield, PA, USA). Size was determined by automated analysis of TEM images using ImageJ (National Institute of Health, Bethesda, MD, USA); at least 500 particles were counted in each population.(Abràmoff et al. 2004) Further details concerning the measurements are summarized in the electronic supplemental material (ESM). Off-line batch-mode DLS and zeta potential measurements were performed using a Zetasizer Nano ZS (Malvern Instruments Inc., Westborough, MA). The characterization of the nanoparticles by batch-mode DLS was performed according to the NIST-NCL protocol (Hackley and Clogston 2007) (see ESM for further details). A4F traces represent the mean of 3–5 replicate injections, where the average coefficient of variation between replicate elutions is less than 1 %. All the reported "mean" size values and plotted hydrodynamic radii, are from either on-line or batch-mode DLS cumulants analysis (i.e., *z*-average hydrodynamic size), and will be noted as r_H or d_H for the radii or the diameter, respectively.

Results and discussion

In this study, optimization of A4F conditions for the fractionation and size determination of positively charged NPs was achieved following a previously developed generalized work flow (Gigault et al. 2014). Validation of the positively charged SeNPs as a calibrant for size and polydispersity is presented, which provides the ability to separate instrumental broadening from sample polydispersity in the A4F channel. Lastly, application of the newly developed A4F methodology for positively charged NPs was applied to CTAB-stabilized AuNPs and a comparison to off-line TEM results is presented.

Characterization of SeNPs

We first present bulk characterization data for a range of SeNP sizes that include samples near the lower and upper limits of detection for the optimized A4F conditions (Table 1), but more intermediate sizes were facilely synthesized by changing the molar ratio of Se and CTAB as described in the experimental section. The PSD determined by batch-mode DLS and TEM diameter PSD for three SeNPs samples are presented in the ESM for comparison (Fig. S1). These three samples represent the lower, an intermediate, and near the upper size limit for on-line characterization. The TEM results are consistent with DLS except

Table 1 Optimal A4F conditions used to fractionate positively charged selenium NPs

Parameters	Optimal conditions
Spacer thickness	250 μm
Mobile phase	0.35 mmol L^{-1} of NH_4NO_3
	0.15 mmol L^{-1} of CTAB
Focus flow	2.0 mL min^{-1}
Focus time	8 min
Injection flow	0.2 mL min^{-1}
Main flow	0.5 mL min^{-1}
Cross flow	1.0 mL min^{-1}

for some divergence in the largest population; this can possibly be attributed to parameterization in the image processing outlined in the ESM or other such artifacts common to analysis by microscopy-based techniques. A more rigorous statistical evaluation was not attempted with TEM, and these results are shown primarily to confirm the uniformity, shape and approximate size of the SeNPs by orthogonal techniques. Additionally, over the entire range of diameters synthesized, the polydispersity index (PI) derived from DLS consistently yielded a value of 0.02 ± 0.01; a PI value well below 0.1 is a strong indicator of monodispersity (ISO 1996). The zeta potential measured for all samples was $\approx +40$ mV, and the pH and ionic strength, I, of the mobile phase was 6.7 and 0.5 mmol L^{-1}, respectively. Combined DLS and TEM results show that all samples of CTAB-coated SeNPs are uniform and (nearly) spherical. Overall, the batch characterization data suggest the CTAB-stabilized SeNPs are an appropriate material for the determination of size-based diffusion and to estimate inherent instrument broadening in hyphenated A4F systems over a broad range of sizes. When purified, these NPs offer sufficient stability (at least one week) and uniformity to calibrate the method.

Calibration for A4F characterization

Due to the absence of commercially available cationic membranes, fractionation, and characterization of positively charged nanomaterials with A4F has not been fully explored nor exploited. To fractionate the positively charged SeNPs, optimization of A4F conditions, including flow rates (channel flow, cross flow, and focus flow), mobile phase concentration and composition, and spacer thickness, is necessary and achieved following a systematic work flow that is presented elsewhere (Gigault et al. 2014).

Here, the optimal mobile phase composition with respect to retention ratio (R, ratio of the void time to t_R at the maximum of the peak), and percent recovery for the fractionation of CTAB-coated SeNPs, was found to be identical to CTAB-coated Au nanorods (AuNRs) previously examined (Gigault et al. 2012). This result provides a consistent determination of ω_{eff} for both Se and Au, and yields direct evidence for the uniformity of the surface of both analyte and membrane when CTAB is incorporated in the mobile phase (Table 1). CTAB in the mobile phase was thought to provide uniformity to the analyte and membrane surfaces, ostensibly mitigating compositional influences of the NPs (e.g., van der Waals forces, surface chemistry, etc.) that have been previously observed to affect retention behavior (Gigault and Hackley 2013). In this previous work an optimal mobile phase composition comprising 0.35 mmol L^{-1} NH_4NO_3 and 0.15 mmol L^{-1} CTAB was determined. This result validates the use of CTAB to mitigate compositional effects, further justifying the use of CTAB-stabilized SeNPs as calibrants potentially for a broad range of positively charged NP analytes, though other ionic surfactants may prove equally effective.

UV/Vis and MALS fractograms of four SeNP populations are shown in Fig. 1, which include the three populations characterized in Fig. S1 and an additional size to further evaluate the size range governed by the optimized conditions (Table 1). It is clearly observed in Fig. 1 that the peaks are separated. Furthermore, sample recovery is >90 % for all samples examined. The on-line DLS enables the hydrodynamic radius ($r_H = ½\ d_H$) to be determined (based on D) across the peak of each SeNP population (see ESM, Fig. S2a). The measured r_H remains fairly constant across the central zone of each peak, confirming the high degree of population monodispersity suggested by TEM and batch-mode DLS. Moreover, due to the optical properties of selenium, the on-line angular dependence of light scattering by the SeNPs yields size information, including the radius of gyration (r_G) and the geometric radius (r), which are derived by the *Zimm* and *sphere* formalisms, respectively; these size parameters are also shown in Fig. 1. The shape of the NPs in each population is characterized by calculating the shape factor, ρ, where $\rho = r_G/$

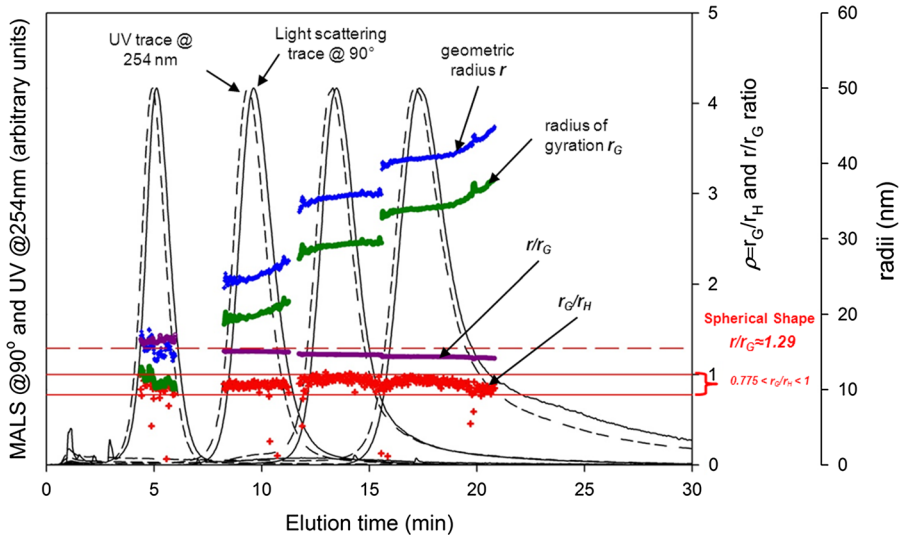

Fig. 1 Representative fractograms for four SeNP populations traced using a single wavelength at 254 nm (*dotted line*) and SLS angle collected at 90° (*solid line*) obtained using fractionation conditions listed in Table 1. The calculated r (*blue*), r_G (*green*) and r_H ratio values are also reported. (Color figure online)

r_H (Burchard 1983). Particles are considered spherical when $0.775 \leq \rho \leq 1$. For all SeNP samples in this study, calculated values for ρ were $\approx$ 1 and represent a sphere. TEM results also demonstrated nearly spherical SeNP cores (Fig. S1), justifying the use of the r model. Together, these data provide validation for the application of the spherical formalism.

To examine the calibration efficiency of SeNPs, the relative standard deviation (RSD, σ) of the calculated effective spacer thickness (ω_{eff}) was determined from the deviation of the linear fit over the broad range examined. A linear relationship between t_R (from the UV–Vis detector trace, that depends on the concentration) and D (from on-line DLS measurements) was observed, resulting in the relationship $t_R = 5.776 \times 10^{-9}/D$ ($R^2 = 0.993$). The RSDs of ω_{eff} obtained for the four points are 1.6, 1.8, 1.1, and 2.7 %, and are within the acceptable range (RSD $< \approx$ 5 %) when compared with other analytical standards used with A4F to characterize NPs from 10 to 100 nm in size (Giddings et al. (1976a)). The low RSD values verify that each individual SeNP calibrant can be used to calibrate ω_{eff}. Consequently, ω_{eff} can be used to back calculate D (i.e., size, in the case of hard sphere NPs) for each sample analyzed under the same conditions using t_R (Eq. S1). The selectivity (S_d) of the optimized conditions is 0.92 (Eq. S2), which is sufficient for separation of the distinct SeNP populations in the channel. By using spherical SeNPs it is possible to obtain a linear relationship between r_H and t_R as illustrated in Fig. 2a. Overall, the on-line measurements provide statistically relevant data demonstrating the uniformity, spherical nature, and applicability of the SeNP sample populations to be used for quantifying the effects of sample broadening in hyphenated A4F systems.

Band broadening in the channel can occur as a result of both polydispersity of the sample and analyte dispersion in the channel stemming from non-equilibrium conditions and axial diffusion. In chromatography, band broadening is related to the theoretical plate height, H, which can be expressed as the summation of these individual contributions (see Eq. S3) and defined as:

$$H = L\left(\frac{\sigma_t}{t_R}\right)^2, \quad (1)$$

where L is the channel length and σ_t represents the standard deviation of the peak measured in units of time. In A4F, several other parameters that can influence band broadening (such as mobile phase, membrane composition, sample nature, etc.) are unaccounted for in Eq. 1, but these contributions are also not dependent on sample polydispersity. Herein, we define instrumental broadening as the summation of the analyte dispersion (band broadening) contributions and other interfacial forces that are not formally described by Eq. 1 but are independent of the analyte size distribution (see "Conclusion" section of the ESM for a more detailed description). If a uniform sample ($\sigma_d \ll d$) is used as a calibrant, the relative contributions to H resulting from only the sample polydispersity, H_p, can be isolated:

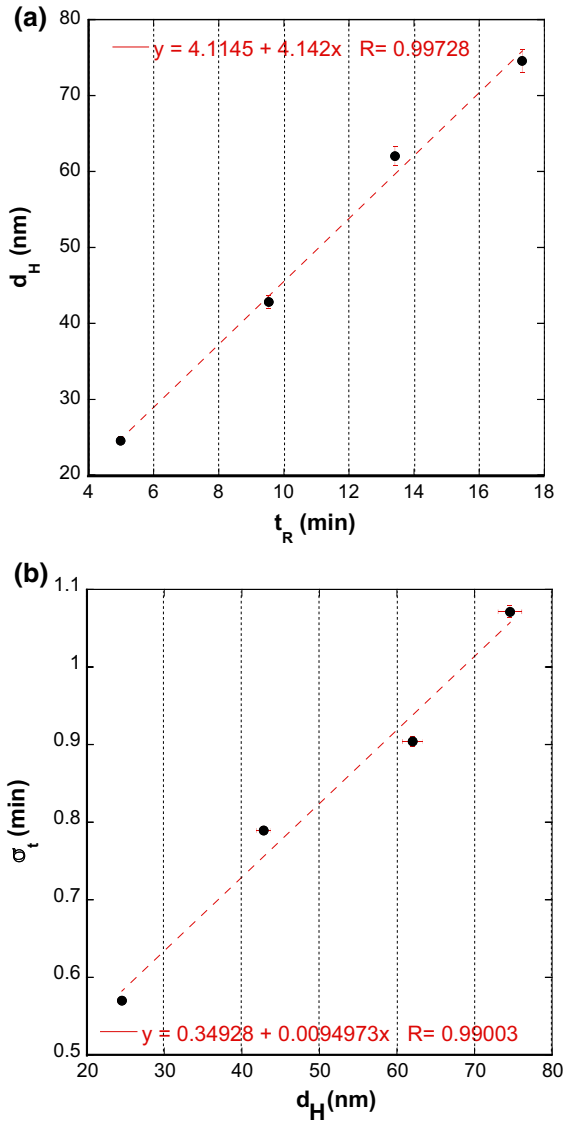

Fig. 2 **a** Dependence of SeNP hydrodynamic diameter on the corresponding t_R measured at the peak maximum with the corresponding linear equation and the associated fit goodness (R); **b** Dependence of σ_t for the SeNP peaks on the mean d_H for the SeNPs

$$H_p = LS_d^2\left(\frac{\sigma_d}{d}\right)^2, \tag{2}$$

where σ_d is standard deviation of the diameter, d (nm). However, in practice, diffusion-based retention is generally applied without consideration of other factors contributing to the peak width, because of the lack of appropriate, well-characterized materials available for quantifying individual contributions for each analyte of interest. The development and implementation of a calibrant *with the same retention behavior in the channel as the analyte* dramatically improves the ability for determining the product distribution of NPs, especially metallic species, with A4F.

The synthesized SeNPs presented in the current work meet the stringent criteria for separating the contributions of band broadening observed in the fractograms (Fig. 1). First, a linear relationship is observed between the standard deviation of the measured retention time, σ_t, for each SeNP population, and the diameter obtained from the on-line light scattering detectors (Fig. 2b); this validates the use of the t_R-based diffusion for determination of the mean diameter. Secondly, the on-line and off-line LS measurements demonstrate the very narrow distribution of species present in each SeNP population, which is also supported by batch DLS and TEM results. Based on the data demonstrating narrow distributions for each SeNP population, we posit that σ_t for each SeNP population is not significantly influenced by sample polydispersity ($\sigma_d \ll d$); therefore, we define σ_t for each SeNP population as σ_t(cal), which represents a variable that is only associated with instrumental and sample broadening effects and not H_p.

Application of the experimental quantification of instrumental broadening in the A4F system *when an appropriate calibrant is employed*, provides a tool to glean more accurate size distribution information than from other commonly used methods. Again, for an unknown sample fractionated in the same conditions as the calibrant, the linear relationship between H and t_R determined for the calibrant will allow determination of the contributing factors to the experimentally observed σ_t, which includes contributions from both sample polydispersity and instrumental broadening. Application of the calibrant allows the difference between the σ_t of the unknown sample, defined as $\sigma_t(x)$, and σ_t(cal), to be determined and defined as $\sigma_t(p)$, which represents the contribution of sample polydispersity of the experimentally measured band width in the unknown sample. Therefore, a new equation for H can be developed that is only related to sample polydispersity, where $H = H_p$ and the information regarding the sample distribution, σ_d, can be determined. Substituting $\sigma_t(p)$ into the A4F plate height equation and solving for σ_d results in:

$$\sigma_d = \frac{d}{t_R S_d}\sigma_t(p) = \frac{d}{t_R S_d}(\sigma_t(x) - \sigma_t(\text{cal})) \tag{3}$$

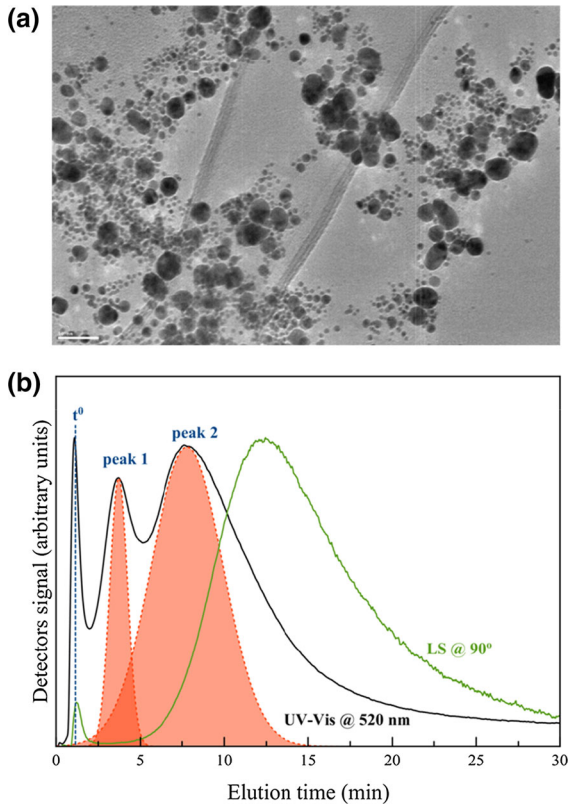

Fig. 3 **a** Representative TEM image of the polydisperse AuNP sample (*scale bar* = 50 nm); **b** A4F-UV–Vis-LS fractograms of the AuNP sample exhibiting two distinct peaks from t_0, centered at 3.0 and 7.9 min. The contribution of the sample polydispersity, $\sigma_t(p)$, for each peak is also plotted (*shaded area*) along with the corresponding light scattering signal collected at 90° (*green*). (Color figure online)

which directly relates the size distribution, σ_d, to the total band broadening observed, σ_t.

Application of the developed methodology based on SeNP calibrants was applied to the well-studied CTAB-coated AuNP system, which results in a broad range of shapes and sizes (e.g., rods and spheres). Importantly, optimization of the CTAB-coated SeNPs demonstrates the mitigating force of the CTAB coating, validating the use of SeNPs as an appropriate calibrant for the CTAB-coated AuNPs. In Fig. 3a, a representative TEM image of the AuNP sample is presented, which provides visual evidence for a polydisperse sample; thus, the sample represents a significant measurement challenge (i.e., determining a statistically relevant size distribution from TEM or common LS techniques would be difficult if not impossible). Implementation of the methodology outlined above enables the distribution of species present in the AuNP sample to be elucidated.

The AuNP sample was investigated with A4F-UV/Vis-MALS and the representative fractograms are shown in Fig. 3b. Examination of the on-line SLS data for the fractionated AuNP species demonstrates the challenges associated with characterizing strongly absorbing, polydisperse samples. First, the on-line DLS data exhibit poor resolution in the autocorrelation function (see ESM, Fig. S4) resulting from the polydispersity of the sample and the short residence time of the analyte in the beam path, introducing bias into the measured size distribution. Second, the onset and shape of the MALS signal at 90° (green trace) is shifted to higher t_R compared to the UV/Vis trace and demonstrates the characterization of the small AuNP populations by LS is intractable for this system. Note the offset in the UV/Vis and LS signals for the polydisperse AuNP sample is in stark contrast to the SeNPs (Fig. 1).

The UV/Vis trace in the fractogram in Fig. 3b exhibits two distinct peaks separated from the void time that are centered at 3 min (peak 1) and 7.9 min (peak 2). Application of the relationship between t_R and d_H established from the spherical SeNP calibrants (Fig. 2a) yields d_H values for the two peaks of 20.0 and 37.6 nm, respectively, which are consistent with the TEM images (Fig. 3a) and provides further supporting evidence for accurate determination of ω_{eff} (Eq. S1) using the SeNP calibrants. By using the linear relationship between σ_t(cal) and d_H from the SeNP calibrants (Fig. 2b) and fitting the two peaks as Gaussian distributions, the contribution from instrumental broadening, σ_t(cal), is subtracted from the raw peak fits to obtain the contribution of the signal resulting only from sample polydispersity, H_p, which are represented as the shaded peak areas in Fig. 3b. Therefore, because the shaded region represents only the contribution of H_p, Eqs. 1 and 2 are used to calculate the resulting σ_d values for peak 1 and peak 2, which yields 3.0 and 10.8 nm, respectively. The determined size distribution is consistent with the global size range and spherical shape observed by TEM. By using an appropriate calibrant that possesses similar retention behavior in the channel, the mean size and the σ_d could be experimentally determined in situ and on-line.

Conclusion

Providing a tool other than microscopy, which requires significant effort in polydisperse systems to be statistically significant and is thus not commonly

achieved (Allen 1981; ISO 2004), begins to address the persistent analytical challenge of developing methods for fast and high throughput post-synthesis characterization of nanomaterials as well as their characterization in more complex systems. Although the size distribution for macromolecules has been determined by A4F, to the best of our knowledge the current work provides the first demonstration for obtaining size distribution information over the entire NP regime detected in the A4F fractogram. Furthermore, as proof of principle, we demonstrated the characterization of a polydisperse CTAB-coated Au species distribution, which are the building blocks for non-zero dimensional materials (e.g., nanorods) and of great interest to nano-medicine and optoelectronic fields (Chithrani et al. 2006; Sandhu et al. 2002). However, current synthetic procedures do not result in a rational synthetic design, instead relying on iterative processing of batch systems, extensive separation procedures and post processing that result in low yields that likely limit commercialization of these promising nanomaterials. The ability to fractionate and characterize distinct populations in these complex, polydisperse systems based on size and shape (aspect ratio) provides a tool to begin elucidating size-dependent behavior, which is important for understanding both synthetic (Chandrasekar et al. 2011) and processing (Gole and Murphy 2004; Grzelczak et al. 2008) pathways in a broad range of systems.

Overall, because CTAB mitigates compositional influences on retention behavior that was previously reported for a broad range of materials in the A4F channel, the development of CTAB-coated SeNP-based calibration standards for metallic nanomaterials was achieved. The uniform monomodal nature of the calibrants allowed instrumental broadening effects in the channel to be quantified and isolated from sample polydispersity, resulting in the ability to determine the NP distribution in polydisperse samples; this requires significant time and effort with other techniques. The SeNPs possess optical properties (efficient scattering, non-plasmonic) that enable accurate characterization of size and structure (shape) and were successfully implemented to determine t_R-based diffusion (size) for cationic AuNPs. Implementation of the SeNP calibrants in the coupled A4F-UV/Vis-MALS system provides a validated tool to probe and characterize a broad range of nanomaterial compositions and sizes in controlled synthetic systems and more complex environments.

Although known for general chromatographic techniques, the current study demonstrates the necessity for validated methods that incorporate appropriate calibrants for determining retention-based diffusion, especially when light scattering methods are intractable, to fully exploit the capabilities of A4F. We believe the current method provides an important tool for probing the contributions of distinct populations of size that can be exploited to develop better synthetic procedures or to evaluate performance in applied NP-based systems. Furthermore, it may be possible to extend this approach using SeNPs as an internal calibrant, where there is clear separation between the SeNP bands and the analyte band, so long as both materials are compatible with the CTAB/NH_4NO_3 mobile phase. In this case, multiple UV/Vis wavelengths or coupling with inductively coupled plasma mass spectrometry may be necessary to identify the calibrant and analyte species. Finally, other surfactants or coatings could be investigated if relevant for extension to other analyte systems.

References

Abràmoff MD, Magalhães PJ, Ram SJ (2004) Image processing with imageJ. Biophotonics Int 11:36–41

Allen T (1981) Particle Size Measurement, 3rd edn. Chapman and Hall, New York

Bendixen N, Losert S, Adlhart C, Lattuada M, Ulrich A (2014) Membrane-particle interactions in an asymmetric flow field flow fractionation channel studied with titanium dioxide nanoparticles. J Chromatogr A 1334:92–100

Brown SC, Boyko V, Meyers G, Voetz M, Wohlleben W (2013) Toward advancing nano-object count metrology: a best practice framework. Environ Health Perspect 121:1282–1291

Burchard W (1983) Static and dynamic light scattering from branched polymers and biopolymers. In: Light scattering from polymers, vol 48. Advances in polymer science. Springer, Berlin and Heidelberg, pp 1–124. doi:10.1007/3-540-12030-0_1

Chandrasekar G, Mougin K, Haidara H, Vidal L, Gnecco E (2011) Shape and size transformation of gold nanorods (GNRs) via oxidation process: a reverse growth mechanism. Appl Surf Sci 257:4175–4179. doi:10.1016/j.apsusc.2010.12.015

Chithrani BD, Ghazani AA, Chan WCW (2006) Determining the size and shape dependence of gold nanoparticle uptake into mammalian cells. Nano Lett 6:662–668. doi:10.1021/nl052396o

Giddings JC (1984) Field-flow fractionation. Separ Sci Technol 19:831–847. doi:10.1080/01496398408068596

Giddings JC, Yang FJ, Myers MN (1976a) Theoretical and experimental characterization of flow field-flow fractionation. Anal Chem 48:1126–1132. doi:10.1021/Ac50002a016

Giddings JC, Yang FJF, Myers MN (1976b) Flow field-flow fractionation—versatile new separation method. Science 193:1244–1245. doi:10.1126/science.959835

Giddings JC, Karaiskakis G, Caldwell KD, Myers MN (1983) Colloid characterization by sedimentation field-flow fractionation. 1. monodisperse populations. J Colloid Interface Sci 92:66–80. doi:10.1016/0021-9797(83)90117-0

Gigault J, Hackley VA (2013) Observation of size-independent effects in nanoparticle retention behavior during asymmetric-flow field-flow fractionation. Anal Bioanal Chem 405:6251–6258

Gigault J, Cho TJ, MacCuspie RI, Hackley VA (2012) Gold nanorod separation and characterization by asymmetric-flow field flow fractionation with UV-Vis detection. Anal Bioanal Chem 405:1191–1202

Gigault J, Pettibone JM, Schmitt C, Hackley VA (2014) Rational strategy for characterization of nanoscale particles by asymmetric-flow field flow fractionation: A tutorial. Anal Chim Acta 809:9–24 doi:http://dx.doi.org/10.1016/j.aca.2013.11.021

Gill R, Lucassen GW (2010) SERRS-based detection of dye-labeled DNA using positively-charged Ag nanoparticles. Anal Methods 2:445–447. doi:10.1039/C0AY00190B

Glover RD, Miller JM, Hutchison JE (2011) Generation of metal nanoparticles from silver and copper objects: nanoparticle dynamics on surfaces and potential sources of nanoparticles in the environment

Gole A, Murphy CJ (2004) Seed-mediated synthesis of gold nanorods: role of the size and nature of the seed. Chem Mater 16:3633–3640. doi:10.1021/cm0492336

Grzelczak M, Sanchez-Iglesias A, Rodriguez-Gonzalez B, Alvarez-Puebla R, Perez-Juste J, Liz-Marzan LM (2008) Influence of iodide ions on the growth of gold nanorods: tuning tip curvature and surface plasmon resonance. Adv Funct Mater 18:3780–3786. doi:10.1002/adfm.200800706

Hackley VA, Clogston JD (2007) Measuring the size of nanoparticles in aqueous media using batch-mode dynamic light scattering. NIST-NCL joint assay protocol PCC-1, Washington, D.C

Hassellöv M, Readman JW, Ranville JF, Tiede K (2008) Nanoparticle analysis and characterization methodologies in environmental risk assessment of engineered nanoparticles. Ecotoxicology 17:344–361

Howard AG (2010) On the challenge of quantifying man-made nanoparticles in the aquatic environment. J Environ Monit 12:135–142

Hutchison JE (2008) Greener nanoscience: a proactive approach to advancing applications and reducing implications of nanotechnology. ACS Nano 3:395–402

ISO (1996) Particle size analysis—photon correlation spectroscopy, 13321. International Standards Organization, Geneva

ISO (2004) Particle size analysis—image analysis methods—Part 1: static image analysis methods, 13322-1. International Standards Organization, Geneva

Lee E, Shon HK, Cho J (2010) Biofouling characteristics using flow field-flow fractionation: effect of bacteria and membrane properties. Bioresour Technol 101:1487–1493

Losert S, Bendixen N, Hungerbühler K, Ulrich A (2013) Membrane—Particle interactions in asymmetric flow field flow fractionation (A4F)—The influence of the ζ-potential. In, 2013. pp 155–158

Ma Y, Guo Y, Li J, Guan J, Xu L, Yang W (2009) Poly(L-lysine)-induced aggregation of single-strand oligo-DNA-modified gold nanoparticles. Chem A Eur J 15:13135–13140. doi:10.1002/chem.200900916

Noskov S, Scherer C, Maskos M (2013) Determination of Hamaker constants of polymeric nanoparticles in organic solvents by asymmetrical flow field-flow fractionation. J Chromatogr A 1274:151–158. doi:10.1016/j.chroma.2012.12.001

Pettibone JM, Gigault J, Hackley VA (2013) Discriminating the states of matter in metallic nanoparticle transformations: what are we missing? ACS Nano 7:2491–2499

Sandhu KK, McIntosh CM, Simard JM, Smith SW, Rotello VM (2002) Gold nanoparticle-mediated transfection of mammalian cells. Bioconjugate Chem 13:3–6. doi:10.1021/bc015545c

Sapsford KE, Tyner KM, Dair BJ, Deschamps JR, Medintz IL (2011) Analyzing nanomaterial bioconjugates: a review of current and emerging purification and characterization techniques. Anal Chem 83:4453–4488

Schimpf ME, Caldwell K, Giddings JC (2000) Field-flow fractionation handbook. Wiley, New York

van Lierop D, Krpetic Z, Guerrini L, Larmour IA, Dougan JA, Faulds K, Graham D (2012) Positively charged silver nanoparticles and their effect on surface-enhanced Raman scattering of dye-labelled oligonucleotides. Chem Commun 48:8192–8194. doi:10.1039/C2CC31731A

Vigderman L, Khanal BP, Zubarev ER (2012) Functional gold nanorods: synthesis, self-assembly, and sensing applications. Adv Mater 24:4811–4841. doi:10.1002/adma.201201690

von der Kammer F, Legros S, Hofmann T, Larsen EH, Loeschner K (2011) Separation and characterization of nanoparticles in complex food and environmental samples by field-flow fractionation. TrAC—Trends Anal Chem 30:425–436

Wei A, Mehtala JG, Patri AK (2012) Challenges and opportunities in the advancement of nanomedicines. J Control Release 164:236–246

Zhang J, Zhang SY, Chen HY (2004) CTAB-controlled synthesis of one-dimensional selenium nanostructures. Chem Lett 33:1054–1055